Fermi level shift in carbon nanotubes by dye confinement

Yann Almadori, G. Delport, Romain Chambard, L. Orcin-Chaix, A. C. Selvati, Nicolas Izard, Anouar Belhboub, Raymond Aznar, B. Jousselme, S. Campidelli, et al.

Fermi level shift in carbon nanotubes by dye confinement

Y. Almadori[(1)], G. Delport[(2)], R. Chambard[(1)], L. Orcin-Chaix[(2)], A.C. Selvati[(3)], N. Izard[(1)], A. Belhboub[(1)], R. Aznar [(1)], B. Jousselme [(4)], S. Campidelli[(4)], P. Hermet[(5)], R. Le Parc[(1)], T. Saito[(6)], Y. Sato[(6)], K. Suenaga [(6)], P. Puech[(7)], J.S. Lauret[(2)], G. Cassabois [(1)], J-L. Bantignies[(1)], L. Alvarez [(1)*]

(1) Laboratoire Charles Coulomb (L2C), CNRS-Université de Montpellier, 34095 Montpellier, F-France.

(2) Laboratoire Aimé Cotton, CNRS, Univ. Paris-Sud, ENS Cachan, Université Paris-Saclay, 91405 Orsay, France

(3) Institut Laue Langevin, BP 156, 38042 Grenoble France

(4) LICSEN, NIMBE, CNRS, Paris-Saclay, CEA Saclay, 91191 Gif-sur-Yvette Cedex, France

(5) Institut Charles Gerhardt Montpellier, CNRS-UM-ENSCM, 34095 Montpellier, F-France

(6) Nanomaterials Research Institute, National Institute of Advanced Industrial Science and Technology (AIST), Tsukuba 305-8565, Japan

(7) Centre d'Elaboration des Matériaux et d'Etudes Structurales (CEMES), UPR-8011 CNRS, Université de Toulouse, Toulouse, France

Abstract: Dye confinement into carbon nanotube significantly affects the electronic charge density distribution of the final hybrid system. Using the electron-phonon coupling sensitivity of the Raman G-band, we quantify experimentally how charge transfer from thiophene oligomers to single walled carbon nanotube is modulated by the diameter of the nano-container and its metallic or semiconducting character. This charge transfer is shown to restore the electron-phonon coupling into defected metallic nanotubes. For sub-nanometer diameter tube, an electron transfer optically activated is observed when the excitation energy matches the HOMO-LUMO transition of the confined oligothiophene. This electron doping accounts for an important enhancement of the photoluminescence intensity up to a factor of nearly six for optimal confinement configuration. This electron transfer shifts the Fermi level, acting on the photoluminescence efficiency. Therefore, thiophene oligomer encapsulation allows modulating the electronic structure and then the optical properties of the hybrid system.

1. Introduction

Hybrid nano-systems, consisting of chromophores confined into the hollow core of single-walled carbon nanotubes (CNT) [1–11] are very exciting materials, not only for their potential applications, but also for the physical interactions taking place in between the two sub-systems. In this context, the new electronic structure of the hybrid system has to be understood properly. Number of investigations have been carried out by DFT calculations [4,12–16]. For instance, DFT calculations suggest that nanotube can modulate electronic and absorption properties of dye oligomers by changing the interchain interactions [13]. It is also predicted that the electronic states added by encapsulated

* laurent.alvarez@umontpellier.fr; 33 4 67 14 35 41

terthiophene molecules to the CNT band structure give rise to optical effects in the radiative relaxation from the excited states of CNT [16]. The calculations also emphasize that the CNT diameter drives the electronic properties of the hybrid system. The ionisation potential of the encapsulated species can be altered by the tube curvature [12] and simulations foresee the appearance of a tiny CT between encapsulated oligothiophenes and CNT when the diameter of the tube is reduced below 1 nm [4]. In contrast, only few experimental works report a qualitative observation of charge transfer (CT) for different types of confined molecules [6,9]. Stable amphoteric doping by encapsulation of organic molecules inside carbon CNT was only shown for a specific tube diameter [9]. A significant CT from the encapsulated oligothiophene to CNT regarding the Raman G band behavior was also reported [6]. Nevertheless, despite all these studies, there is no experimental quantification of this charge transfer and key parameters such structural and electronic properties of CNT are not taken into account.

To experimentally address this question, we present here a joint Raman and photoluminescence study of the confinement of dimethyl-quaterthiophenes (4T), inside single-walled carbon nanotubes, revealing charge transfers which depend on the CNT diameter and its electronic properties (metallic or semiconducting).

2. Experimental Section

2.1 Sample Preparation

Four sources of CNT were used in this study. Commercial electric arc single-walled carbon nanotubes (1.2 nm < *diameter* < 1.6 nm) and called CNT14 in the following. Two kinds of CNT14 were used: (1) purified and annealed MEIJO nanotubes from Meijo Nano Carbon (http://www.meijo-nano.com/en/) and (2) highly functionalized (called defective in the following) nanotubes from carbon solution (http://www.carbonsolution.com/products)[17]. Carbon CNT synthesized by the eDIPS method[18] (1.6 nm < *diameter* < 2 nm) (CNT17 in the following) are also studied. CoMoCAT carbon nanotubes[19] enriched in (7,6) nanotubes (0.6 nm < *d* < 1 nm), (www.sigmaaldrich.com/) called CNT09 in the following are also used. Carbon Solution and CoMoCAT CNT were purified by air oxidation and subsequently treated to remove the catalyst. The CNT17 nanotubes were purified according to the method previously described[11].

Encapsulation of dimethyl-quaterthiophene ($C_{18}H_{14}S_4$) into carbon nanotubes was performed using the vapor reaction method previously described[6]. The hybrid material is named 4T@NTXX in the following where XX represents the mean diameter (09, 14 or 17 Å). The reference pristine nanotubes (NTXX) have undergone the same thermal treatments as the hybrid sample during the encapsulation process. Encapsulation was probed by TEM and x-ray diffraction (Figure 1 & 2 of SM).

* laurent.alvarez@umontpellier.fr; 33 4 67 14 35 41

2.2 Raman Spectroscopy

Micro Raman experiments have been performed on a triple monochromator spectrometer (Jobin Yvon T64000), equipped with a charge-coupled detector, in a backscattering geometry, using the fixed 413.0, 457.9, 488.0, 501.0, 514.5, 521, 532.0, 568.2, 647.1 and 660.0 nm excitation wavelengths. In order to prevent the heating of the tubes and oligomers, the laser power was adjusted at 200 μW. This laser power is less than half the power causing a variation of the Raman spectrum. The spot diameter is of about 3 μm using a 50× objective. The resolution is about 2 cm^{-1}. At least five spatially separated areas of each sample were probed to ensure homogeneity.

2.3 Annular dark-field scanning TEM (ADF-STEM) and SR-EELS

4T@NT samples were dispersed in *n*-hexane by ultrasonication, and dropped onto molybdenum microgrids coated with holey amorphous carbon films for analyses by annular dark-field scanning TEM (ADF-STEM). A JEOL JEM-2100F electron microscope equipped with double JEOL Delta spherical aberration correctors was operated at an electron accelerating voltage of 60 kV for STEM observation. Spatially-resolved Electron energy-loss spectroscopy (SR-EELS) measurement was carried out using a Gatan Quantum electron spectrometer attached to the microscope. Elemental distributions of carbon and sulfur in individual CNTs were determined based on the intensities of their K and L edges, respectively, at each measured point in the scanned areas by STEM-EELS chemical mapping.

2.4 Photoluminescence spectroscopy

Photoluminescence Excitation (PLE) spectroscopy was performed using a home-made PL setup. The output of a Xe lamp was monochromated and focalised on the sample. PL is recorded with a 320 mm spectrometer and 150 lines/mm grating, and detection is performed by a nitrogen-cooled 512 pixel linear InGaAs array. Pristine and encapsulated CNTs were suspended in aqueous solvent using sodium cholate surfactant by sonication using a microson ultrasonic cell disruptor Misonix XL2000 for 20 min at 50% followed by ultracentrifugation at 120 kg for 30 min.

3. Results

3.1 ADF-STEM and SR-EELS

STEM-EELS studies were performed on all the hybrid nanotubes under investigation to ascertain the 4T encapsulation efficiency[11]. Figures 1.a,b,c display a ADF-STEM images of 4T into small diameter (~9 Å) CNT (4T@NT09), see experimental section).

* laurent.alvarez@umontpellier.fr; 33 4 67 14 35 41

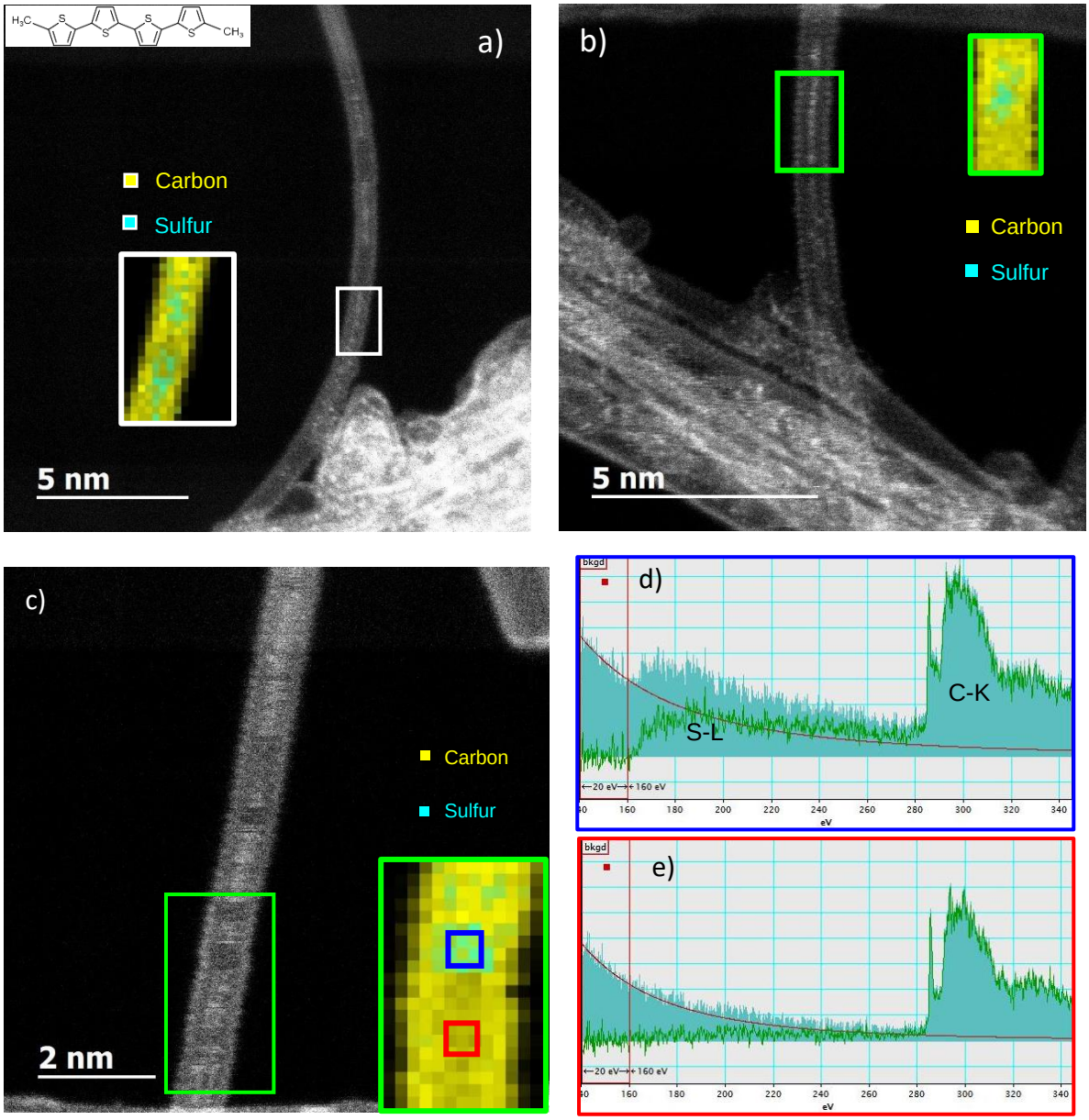

Figure 1: ADF-STEM images of a 4T@NT09 nanotubes and superimposed carbon (yellow) and sulfur (green) elemental maps. Two EEL spectra (d,e) extracted from the marked areas showing K edge of carbon (~ 284 eV) and $L_{2,3}$ edge of sulfur (~165–220 eV) only in (d). Inset in a) Structure of 4T.

A clear contrast is observed inside the tube, indicating that they are filled. Additionally, SR-EELS experiments were carried out to unveil the chemical nature of the confined species and their localization. The highlighted area (green square) in Figures 1 a,b,c corresponds to a domain where EELS measurements have been performed. Figures 1.d,e show two EEL spectra recorded in the marked areas in Figure 1.c. The energy loss near-edge features (ELNES) of the carbon K edge (C–K), which consists of a π* peak at ~285 eV and a well-defined σ* band starting at ~292 eV, are present in both EEL spectra. The S–$L_{2,3}$ edge, which consist of a rather large peak around 165–220 eV, is clearly visible only in Figure 1.d. It appears that sulfur (from 4T) is not surrounding the

* laurent.alvarez@umontpellier.fr; 33 4 67 14 35 41

nanotubes but is mainly localized within the hollow core of the tubes giving thus insights on the quality of the encapsulation procedure.

3.2 Raman measurements

Raman spectroscopy is used to probe pristine CNT and hybrid 4T@NT in order to investigate the physical interactions taking place between the confined molecules (4T) and the host nanotubes.
The G^- and G^+ (lying from 1500 to 1595 cm^{-1}) modes correspond respectively to the circumferential–transverse (TO) and the longitudinal (LO) optical modes [20] of semiconducting CNT (Sc_CNT). For metallic tubes (M_CNT), a Kohn anomaly (vibrations are partially screened by electrons [21]) strongly reduces the LO frequency and significantly modifies the profile of the mode. Thus, the G^- and G^+ bands are respectively assigned to the LO and TO modes [22]. The LO mode (for both Sc_CNT or M_CNT) is particularly sensitive to changes in the electronic structure, making it as a powerful tool to probe CT.

3.2.1. Hybrid systems with semiconducting nanotubes

The G-band behavior for semiconducting CNT upon CT can be described as follow:

- For narrow diameter semiconducting CNT, static n (p)-type doping respectively reduces (increases) the force constants by adding (or removing) electrons on the bonding, leading respectively to a softening or a hardening of the G^+ band [23–25]. In this case, the magnitude of the shift can be derived from the following relationship adapted from [23] or [25] :

$$\Delta\omega_{static}(cm^{-1}) = -804\times\rho_c - 5126\times\rho_c^2 - 176790\times\rho_c^3 - 1657\times\rho_c^{3/2} \quad (1)$$

where ρ_c is the number of electron transferred per carbon atom of the nanotube [25].

- For large diameter semiconducting CNT, because of the narrow energy bandgap, an EPC takes place, reducing the vibration frequency of pristine nanotubes. Upon CT, the Fermi level downshifts or upshifts (for hole and electron transfer respectively), modifying EPC and leading to a systematic upshift of G-band position (named renormalization effect)[26] whatever the kind of doping (n or p type)[25,26].

Finally, for all kind of tubes, once ρ_c is determined, the Fermi level shift can be estimated for weak charge transfer with the following equation, adapting the equation below from Ref. [27]:

$$\Delta E_F(eV) = 51.77 \times \rho_c \times d(nm) \qquad (2)$$

where *d* is the CNT diameter.

Therefore, a careful analysis of the Raman LO G-band after 4T encapsulation is a powerful tool to investigate the CT and the Fermi level shift.

* laurent.alvarez@umontpellier.fr; 33 4 67 14 35 41

Figure 2 displays the high energy modes of the pristine CNT (black curves) and 4T@NT nanosystems (blue curves) for different CNT diameters measured at different excitation wavelengths. Other spectra are shown in figure 3 of SM. The spectra exhibit the G-bands of the nanotubes (G^- and G^+ lying from 1500 to 1595 cm^{-1}) and the C=C stretching vibrations of the confined 4T (around 1440-1530 cm^{-1}).

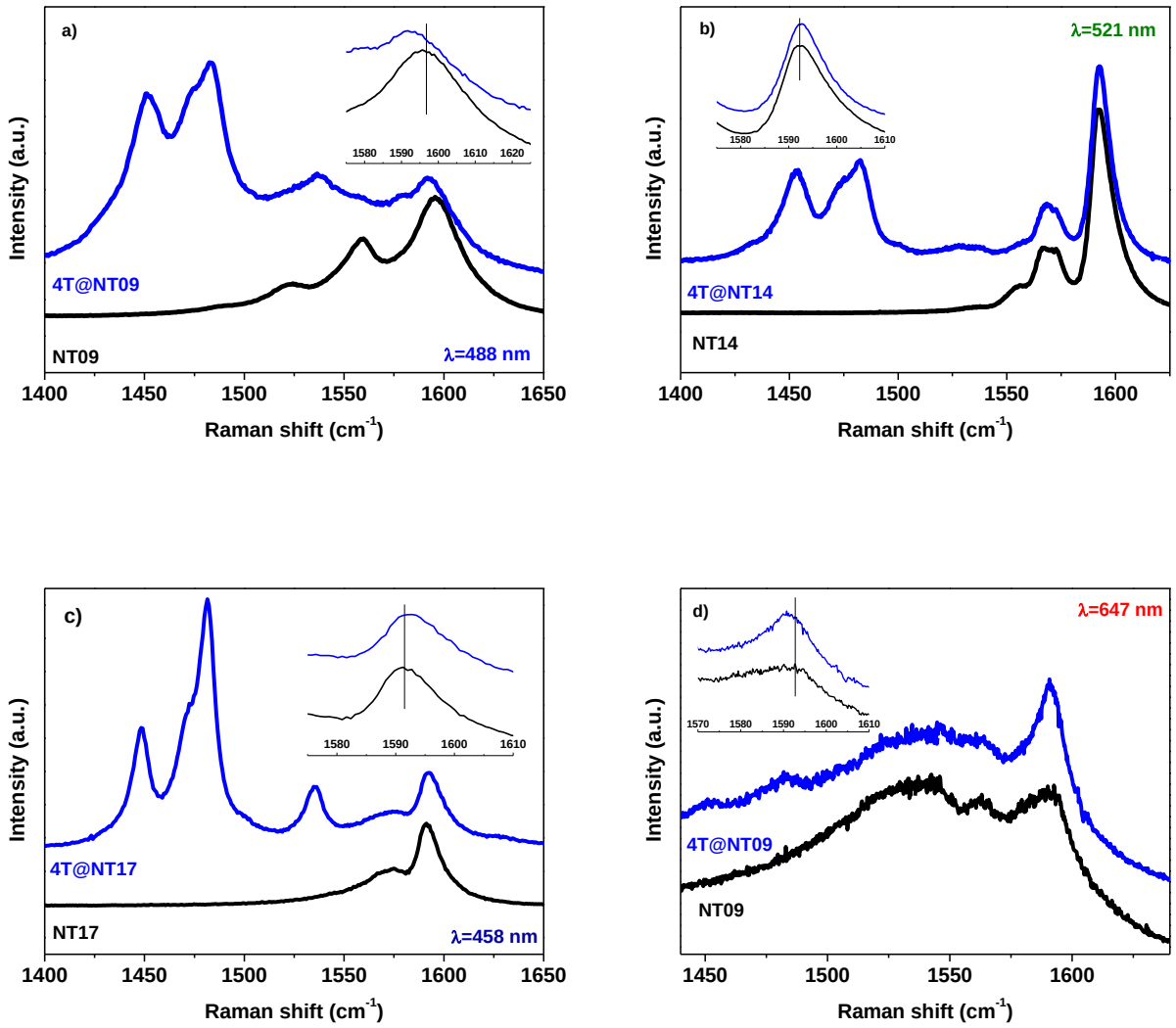

Figure 2: *Raman spectra of pristine (black curve) and hybrid (blue curve) nanotubes of different diameters excited at different excitation wavelengths. Hybrid spectra are offset for clarity.*

We can observe significant changes both in position (inset Fig.2) and profile after 4T encapsulation. It is worth to mention that the magnitude and the direction (upward or downward) of the G-band shifts strongly depend on the CNT diameter (Inset Fig.2 and Fig.4 SM). Figure 3 displays the relative G^+ band shifts of the hybrid systems with respect to pristine Sc_CNT as a function of several excitation wavelengths for the three different CNT diameters (NT09, NT14 and NT17) considered in this work. This G^+ band corresponds to the LO mode of Sc_CNT. We can clearly observe a significant downshift for small diameter tubes (NT09, blue circle), consistent with a static effect (change in a

* laurent.alvarez@umontpellier.fr; 33 4 67 14 35 41

lattice spacing) due to an electron transfer (E_LT) from the 4T. By contrast, larger diameter tubes (NT14 and NT17, wine triangle and black square respectively) exhibit a slight upshift, consistent with a dynamic effect (renormalization).

The Raman G-bands are very sensitive not only to charge transfer but also to different environmental effects such as temperature [28,29], strain [28,30,31] and pressure [32]. However, these effects shift the G^+ band in the same direction independently on the CNT diameter, unlike the results displayed on figure 3. In addition, no G^+-band shift has been reported for encapsulated molecules giving rise to van der Waals interactions with CNT [33,34]. Therefore, the G+ band behavior for the three diameters under investigations and for all excitation wavelengths are interpreted in terms of E_LT from the confined 4T to the host CNT, neglecting all other effects.

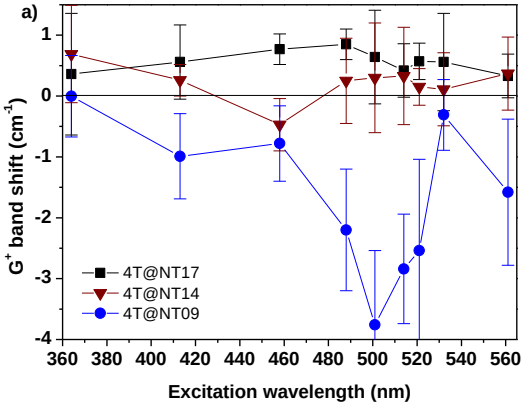

Figure 3: *Raman G^+-band shifts of Sc_NT after 4T confinement as a function of the excitation wavelength for 4T@NT17 (black square), 4T@NT14 (wine triangle) and 4T@ NT09 (blue circle).*

For small diameter tubes (NT09), according to equation (1), shifts in the range from -0.28 cm^{-1} to -1.6 cm^{-1} corresponds to $\rho_c \sim (1.1\pm0.7)\times10^{-3}$. Considering then a length of the 4T molecule around 2 nm and calculating the number of carbon atoms in a CNT of the same length with a diameter of 9 Å, this value suggests $\rho_{4T}=0.25\pm0.15$, (ρ_{4T} is the number of electron withdrawn from one 4T molecule) and assuming that only one 4T molecule is inserted into a NT09 section [11]. Considering equation (2), the Fermi shift $\Delta E_F=0.05\pm0.03$ eV for 4T@NT09.

Thus, for Sc_CNT, the E_LT seems more important for small diameter (NT09) with respect to larger tubes (NT14), in good agreement with our DFT calculations (Fig.5 SM).

Furthermore, an important amplification of the downshift for excitation wavelengths between 488 and 521 nm is evidenced. As the optical absorption of the confined 4T molecules lies in this energy range, we can reasonably assume an additional photo-induced CT, leading to a larger G-band downshift (from -2.2 cm^{-1} to -3.7 cm^{-1}), corresponding to $\rho_c \sim (3.2\pm0.8)\times10^{-3}$ and $\rho_{4T}=0.73\pm0.17$.

* laurent.alvarez@umontpellier.fr; 33 4 67 14 35 41

Here, ΔE_F=0.15±0.04 eV for 4T@NT09 at the molecule resonance. This photo-activated CT has been observed with porphyrin molecules deposited on the outer surface of double walled carbon nanotubes [35]. Then, the redox state of the molecule under light irradiation is assumed to be stable overs hours. For larger diameter tubes (NT14 and NT17), the slight upshift (roughly constant over the excitation wavelength range) indicates that dynamic effects dominate the G-band behavior. Considering calculations on graphene [23], on individual semiconducting CNT [26] or measurements on an ensemble of CNT [36], the magnitude of the upshifts observed on figure 3 from +0.11 cm^{-1} to +0.37 cm^{-1} (for NT14) can be explained by an E_LT such as $\rho_c \sim (0.6\pm0.3)\times10^{-3}$ and ρ_{4T}=0.10±0.05 (assuming that two 4T molecules are inserted in the CNT section of such a diameter [11]). The Fermi level shift is then estimated as ΔE_F=0.045±0.025 eV for 4T@NT14.

3.2.2 Hybrid systems with metallic nanotubes

For metallic CNT, a Kohn anomaly (vibrations are partially screened by electrons [21]) due to EPC, strongly reduces the LO frequency and changes the profile of the mode. This coupling, between the electronic continuum and the discrete vibrational states, induces for the LO mode an asymmetric Breit-Wigner-Fano (BWF) line shape [37] (green cross of figure 4), described by the following equation:[37,38]

$$I(\omega) = I_0 \frac{[1+(\omega-\omega_{BWF})/q\Gamma]^2}{[1+(\omega-\omega_{BWF})/\Gamma]^2} \quad (3)$$

where 1/q measures the strength of the interaction, ω_{BWF} is the peak frequency at maximum intensity I_0 and Γ the spectral width.

Therefore, upon CT, the G^- band frequency and lineshape of metallic CNT are significantly modified.

Figure 4 displays the Raman G bands of CNT14, NT14 defective nanotube (NT14_D, D stands for defect), and 4T@NT14_D using a red excitation wavelength (660 nm), allowing to probe M_NT14 [38]. The defective CNT (NT14_D) are not annealed after the purification step, giving rise to several functional groups (C-OH, C=O, COOH…) remaining at their outer surface.

The BWF line shape of the Raman G^--band observed for non-defective tubes (green cross) and signing an important EPC [38], is strongly modified for defective nanotubes (black open circle). Considering that surface defects induce a p-type doping of the tube [39], the downshift of E_F weakens the EPC, thus upshifting the G^- modes [26]. After 4T encapsulation (blue triangle), the peculiar BWF profile is recovered. This phenomenon is interpreted as a consequence of E_LT from the confined molecule to the nanotube, shifting back E_F (balancing out the p-type doping from defects) and reducing the phonon energy by a strengthening of the EPC. This is another clue emphasizing the CT from 4T encapsulation is given by the study of defective metallic CNT.

* laurent.alvarez@umontpellier.fr; 33 4 67 14 35 41

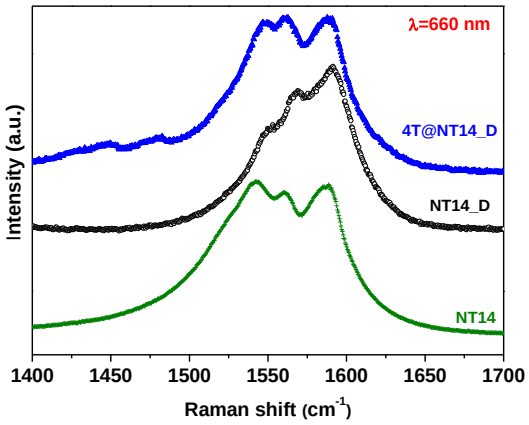

Figure 4: *Raman spectra of annealed M_CNT14 (green cross), defective nanotube CNT14_D (open circle) and hybrid 4T@NT14_D (blue triangle)*

The next step is to obtain a quantitative information on the CT between the encapsulated 4T and CNT from the G-band shifts. To this aim, we compare our experimental results to theoretical models developed either for graphene [23] and/or metallic CNT [26,27,36,40]. Some of these calculations are combined to measurements on individual CNT [26,27,40] or an ensemble of CNT [36]. It is worth to mention that, fortunately, the CT estimation from our data does not strongly depend on the chosen model.

Several Raman spectra of metallic NT14 and 4T@NT14 samples recorded with different excitation wavelengths (633, 638, 647 and 660 nm) have been fitted using a BWF equation (Fig.6 SM) to study the coupling after 4T encapsulation.

The fitting parameters (Fig.5) for the different excitation wavelengths evidence a weakening of the EPC after 4T encapsulation as the coupling factor -1/q decreases from -0.20 down to -0.10, concomitant with a G^--band upshift $\Delta\omega_{BWF}$ of around 3 cm^{-1} in average and a narrowing of the peak width Γ for about 4 cm^{-1}. All modifications are consistent with a weakening of EPC [40].

Considering studies on individual CNT, the frequency shifts suggest an E_LT per carbon atom of CNT of $\rho_c \sim (1.8\pm0.4)\times10^{-3}$ ($\rho_{4T}\sim0.30\pm0.07$) [26], giving $\Delta E_F=0.14\pm0.03$ eV. Considering now the experimental work by A. Das et al. [36], performed on an ensemble of CNT, the peak widths and the frequency shifts are given as a function of the Fermi level shift. Comparing our values in Fig.5.a (top and bottom) to their data, one can estimate $\Delta E_F=0.16\pm0.4$ eV in our 4T@NT14, giving rise to $\rho_c\sim(2.3\pm0.6)\times10^{-3}$ and $\rho_{4T}=0.32\pm0.03$. Finally, it is worth mentioning that the decrease by a factor of 2 of the coupling parameter -1/q (Fig.5.a, middle) has been already observed on individual nanotube

* laurent.alvarez@umontpellier.fr; 33 4 67 14 35 41

of similar diameter (1.2 nm) and associated to a Fermi level shift ΔE_F~0.2 eV, in rather good agreement with our measurements.

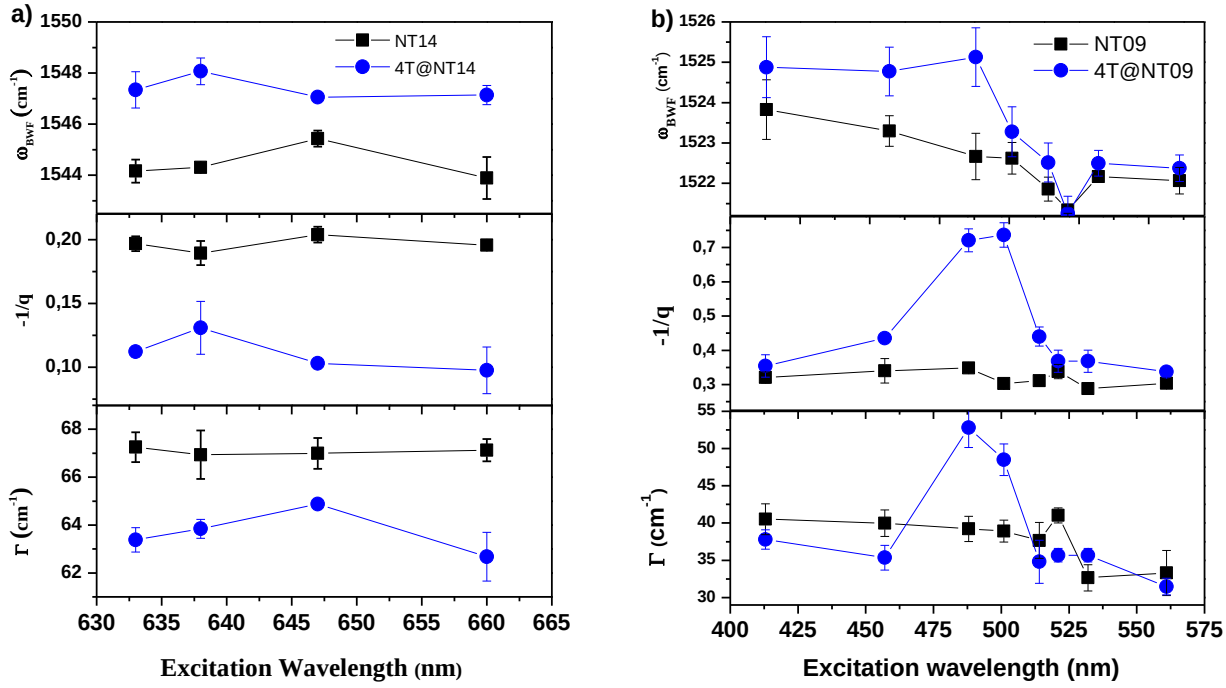

Figure 5: a) ω_{BWF} (top), -1/q (middle) and Γ (bottom) values for NT14 (black square) and 4T@NT14 (blue circle) as a function of excitation wavelengths. b) ω_{BWF} (top), -1/q (middle) and Γ (bottom) values for NT09 (black square) and 4T@NT09 (blue circle) as a function of excitation wavelengths.

We also investigate the G$^-$-band (metallic LO mode) behavior undergoing the EPC and exhibiting a BWF line shape to probe metallic small diameter NT09. The situation is significantly different from the case of NT14 for at least two reasons: i) to probe metallic NT09, excitation wavelengths in the 450-550 nm range are required, corresponding to the absorption window of the 4T (leading to resonance conditions of the confined molecules; ii) the gap opening due to CNT curvature [41,42] is no longer negligible [27].

Fitting the Raman modes for both pristine CNT and hybrid system 4T@NT09 (figure 7 SM), we calculate -1/q, $\Delta\omega_{BWF}$ and Γ. Figure 5.b displays the fitting parameters as a function of the excitation wavelengths. Out of the resonance window of the encapsulated molecule, we firstly notice very slight difference between empty NT09 and 4T@NT09, meaning that metallic NT09 are hardly altered by the interaction with the 4T. By contrast, within the resonance window, one can clearly observe after 4T confinement a strong enhancement of the coupling factor -1/q, a decrease of Γ and a slight upshift of the frequency whose magnitude depends on the excitation wavelength. Thus, for NT09, the 4T confinement rather strengthen the asymmetry of the EPC. These behaviors are consistent with a

* laurent.alvarez@umontpellier.fr; 33 4 67 14 35 41

significant photo-activated charge transfer as the energy range matches the 4T absorption. According to literature, this suggests that the photo-excited electrons coming from the encapsulated 4T mostly contribute to the asymmetry of the G^--band due to electron-electron interactions [43,44].

3.3 Photoluminescence measurements

Figure 6 exhibits the photoluminescence excitation (PLE) maps of both NT09 (Fig. 6.a) and hybrid 4T@NT09 (Fig.6.b). For this diameter distribution, only one 4T molecule is inserted into a nanotube section. On these PLE maps one can see that after 4T encapsulation both E_{22} and E_{11} CNT transition energies (between symmetric van Hove singularities) are shifted. In addition, a significant increase of the photoluminescence intensity is generally observed. Indeed, figure 7.a shows that the PL intensity ratio derived from figure 5 ($I_{4T@NT09}/I_{NT09}$) increases with the nanotube diameter. Note that here the intensities have been normalized by adjusting the absorption intensity on the E_{22} transitions of both samples (fig.8 SM). (6, 5) CNT shows an intensity ratio close to unity as its diameter is too narrow to incorporate a 4T molecule. On the contrary, a ~5.5 increase of PL intensity is observed for the (9, 4) nanotube. This shows that the encapsulation of 4T molecules allows to tune the emission properties of these small diameter CNT. This behavior has also been observed for ferrocene or alkane encapsulation [45,46]. Moreover, a similar diameter dependence of the PL intensity was already observed when nanotubes undergo a strong external electric field [47]**.** Larger diameter tubes with smaller bandgap would be more altered as their exciton binding energy is reduced. In our case, the increase of the intensity could be explained by the weak electron transfer from the confined 4T molecule to the CNT compensating the natural p-type doping of pristine nanotubes due to curvature [48], defects [49]… Thus, the charge transfer moves back the Fermi level closer to its expected position for "perfect" tube [45], increasing the PL efficiency when the size of the nano-container increases. The maximum PL intensity is reached for an optimized tube diameter of 0.92 nm, here (9,4). The following drop for the (8,6) nanotubes can be interpreted with two hypothesis 1) a progressive negative charge transfer from 4T after natural p doping compensation or 2) a change of chromophore environment, 4T favoring π-type interaction with the nanotube walls when its diameter increases. As mentioned above, both E_{22} and E_{11} transitions of filled nanotubes are shifted with respect with empty nanotubes.

Figure 9 of SM displays the energy shifts the E_{22} (blue square) and E_{11} (red circle) for 4T@NT09 with respect to NT09. It shows that (7,5) and (8,4) nanotubes exhibit red shifts up to 30-40 meV. These behaviors have been also observed when asymmetric dyes molecules or alkanes are encapsulated in small diameter nanotubes [2,46]. Among the potential origins of these shifts, mechanical strain and dielectric screening have to be considered. Moreover, it turns out that mechanical strain leads to energy shifts with the same amplitude but with opposite signs for the E_{11}

* laurent.alvarez@umontpellier.fr; 33 4 67 14 35 41

and E_{22} transitions [50]. Furthermore, if one considers that the difference of exciton screening due to the encapsulation of 4T molecules is of the same amplitude and sign for both E_{11} and E_{22} transitions, as it is the case for changes in the surrounding environment, one can separate the contributions of screening and strain (see SM) [51].

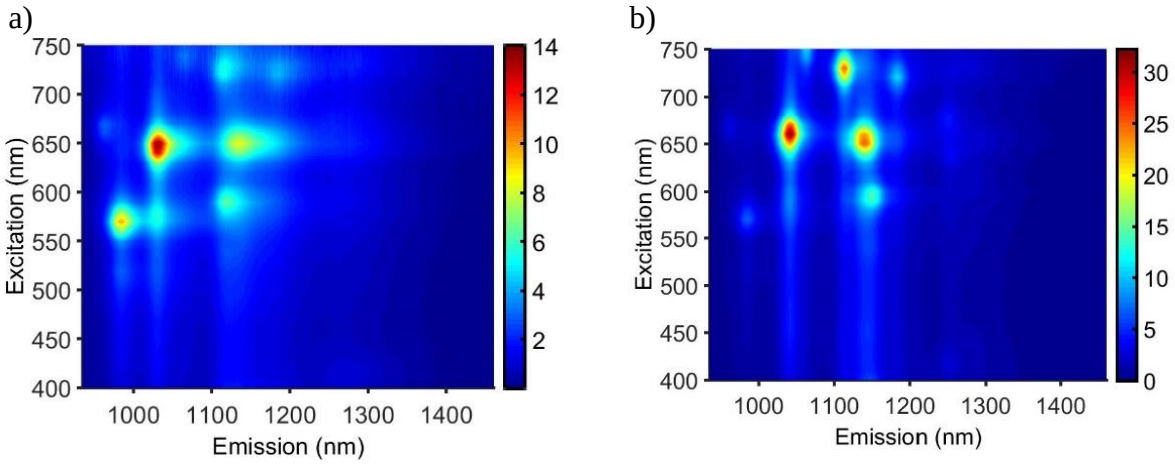

Figure 6*: PL signal intensity versus emission (x-axis) and excitation (y-axis of NT09 (a) and 4T@NT09 (b)*

Figure 7.b exhibits the results obtained for our small diameter tubes. We can clearly identify two distinct behaviors, considering that the (6,5) nanotube is probably empty because of its narrow diameter preventing molecule encapsulation.

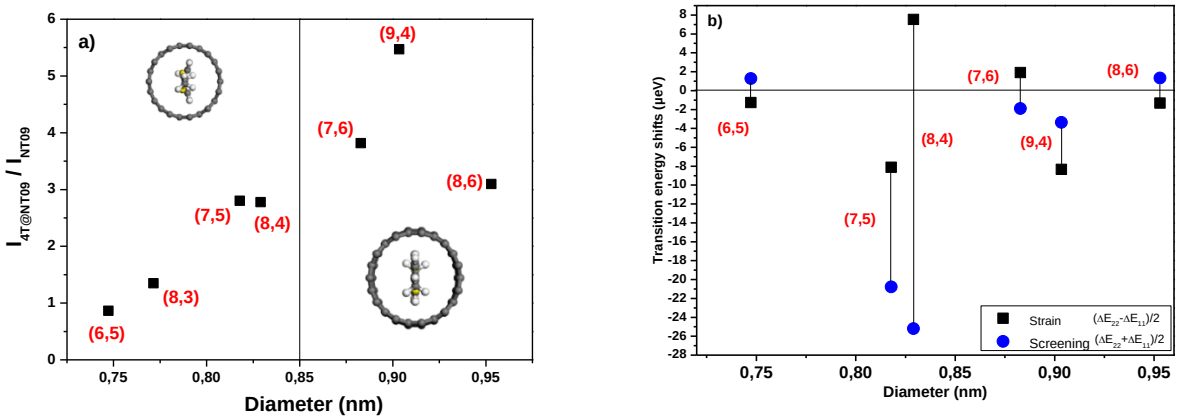

Figure 7*: a) PL intensity ratio between 4T@NT09 and NT09 as a function of CNT diameters*
b) Mechanical and electronic contributions of the PL energy shifts for 4T@NT09 with respect to NT09

The (7,5) and (8,4) nanotubes undergo both mechanical strain and screening effects whereas larger diameter tubes (from (7,6) to (8,6)) display rather small shifts indicating no important changes with respect to the empty nanotubes. These behaviors are very reasonably assigned to the local structures predicted from DFT calculations and illustrated by two schemes in figure 6a. For very small diameter tubes (below 0.86 nm corresponding to minimum diameter allowing 4T encapsulation), the 4T molecule is incorporated but induces constraints on the nanotube and leads to mechanical strains. In

* laurent.alvarez@umontpellier.fr; 33 4 67 14 35 41

contrast, on large diameter tubes, the molecules are located near the center of the tube with only weak mechanical constraints [52]. Moreover, the sign of the strain induced shift depends also on q=n-m mod(3). Therefore, the (7, 5) nanotubes with q=-1 and the (8, 4) nanotubes with q=1 should exhibit strain induced shifts with opposite sign [50]. This is exactly what is shown on figure 10, thus reinforcing our interpretation.

4. Conclusions

In summary, significant electron transfer from confined quaterthiophene derivatives to single-walled carbon nanotubes is evidenced. The amount of exchanged electrons strongly depends on the nanotube diameter and its metallic or semiconducting character. In addition, a photo-activated transfer takes place for small diameter tube when the excitation wavelength matches the 4T absorption. Different behaviors are observed for metallic nanotubes with different diameters. For small diameters (NT09), the coupling factor increases within the resonance window of the 4T, featuring a strengthening of the electron-phonon coupling. In contrast, for large diameter tubes, this factor is reduced out of the resonance, consistent with a weakening of the coupling. This charge transfer leads also to an important enhancement of the photoluminescence intensity of small diameter tubes by a factor up to six. This effect is assigned to a n-type doping balancing out the natural p-type doping of small diameter tubes due to defects or σ-π orbital hybridization. This study allows an experimental quantification of the charge transfer from confined quaterthiophene to host carbon nanotube as a function of key parameters such as diameter, and electronic character (metallic or semiconducting) of nanotube.

Acknowledgements:

L.A would like to acknowledge F. Neumayer, S. Moyano and G.X. Chan for their helps in Raman measurements. The authors also thanks the IRRAMAN platform of the university of Montpellier for providing access to the Raman apparatus.

References:

[1] E. Gaufrès, N.Y.-W. Tang, F. Lapointe, J. Cabana, M.-A. Nadon, N. Cottenye, F. Raymond, T. Szkopek, R. Martel, Giant Raman scattering from J-aggregated dyes inside carbon nanotubes for multispectral imaging, Nature Photonics. 8 (2013) 72–78. doi:10.1038/nphoton.2013.309.

[2] S. Cambré, J. Campo, C. Beirnaert, C. Verlackt, P. Cool, W. Wenseleers, Asymmetric dyes align inside carbon nanotubes to yield a large nonlinear optical response, Nature Nanotechnology. 10 (2015) 248–252. doi:10.1038/nnano.2015.1.

* laurent.alvarez@umontpellier.fr; 33 4 67 14 35 41

[3] M.A. Loi, J. Gao, F. Cordella, P. Blondeau, E. Menna, B. Bártová, C. Hébert, S. Lazar, G.A. Botton, M. Milko, C. Ambrosch-Draxl, Encapsulation of Conjugated Oligomers in Single-Walled Carbon Nanotubes: Towards Nanohybrids for Photonic Devices, Advanced Materials. 22 (2010) 1635–1639. doi:10.1002/adma.200903527.

[4] J. Gao, P. Blondeau, P. Salice, E. Menna, B. Bártová, C. Hébert, J. Leschner, U. Kaiser, M. Milko, C. Ambrosch-Draxl, M.A. Loi, Electronic Interactions between “Pea” and “Pod”: The Case of Oligothiophenes Encapsulated in Carbon Nanotubes, Small. 7 (2011) 1807–1815. doi:10.1002/smll.201100319.

[5] E. Gaufrès, N.Y.-W. Tang, A. Favron, C. Allard, F. Lapointe, V. Jourdain, S. Tahir, C.-N. Brosseau, R. Leonelli, R. Martel, Aggregation Control of α-Sexithiophene *via* Isothermal Encapsulation Inside Single-Walled Carbon Nanotubes, ACS Nano. 10 (2016) 10220–10226. doi:10.1021/acsnano.6b05660.

[6] L. Alvarez, Y. Almadori, R. Arenal, R. Babaa, T. Michel, R. Le Parc, J.-L. Bantignies, B. Jousselme, S. Palacin, P. Hermet, J.-L. Sauvajol, Charge Transfer Evidence between Carbon Nanotubes and Encapsulated Conjugated Oligomers, The Journal of Physical Chemistry C. 115 (2011) 11898–11905. doi:10.1021/jp1121678.

[7] K. Yanagi, K. Iakoubovskii, H. Matsui, H. Matsuzaki, H. Okamoto, Y. Miyata, Y. Maniwa, S. Kazaoui, N. Minami, H. Kataura, Photosensitive Function of Encapsulated Dye in Carbon Nanotubes, Journal of the American Chemical Society. 129 (2007) 4992–4997. doi:10.1021/ja067351j.

[8] K. Yanagi, K. Iakoubovskii, S. Kazaoui, N. Minami, Y. Maniwa, Y. Miyata, H. Kataura, Light-harvesting function of β -carotene inside carbon nanotubes, Physical Review B. 74 (2006). doi:10.1103/PhysRevB.74.155420.

[9] T. Takenobu, T. Takano, M. Shiraishi, Y. Murakami, M. Ata, H. Kataura, Y. Achiba, Y. Iwasa, Stable and controlled amphoteric doping by encapsulation of organic molecules inside carbon nanotubes, Nature Materials. 2 (2003) 683–688. doi:10.1038/nmat976.

[10] L. Alvarez, F. Fall, A. Belhboub, R. Le Parc, Y. Almadori, R. Arenal, R. Aznar, P. Dieudonné-George, P. Hermet, A. Rahmani, B. Jousselme, S. Campidelli, J. Cambedouzou, T. Saito, J.-L. Bantignies, One-Dimensional Molecular Crystal of Phthalocyanine Confined into Single-Walled Carbon Nanotubes, The Journal of Physical Chemistry C. 119 (2015) 5203–5210. doi:10.1021/acs.jpcc.5b00168.

[11] Y. Almadori, L. Alvarez, R. Le Parc, R. Aznar, F. Fossard, A. Loiseau, B. Jousselme, S. Campidelli, P. Hermet, A. Belhboub, A. Rahmani, T. Saito, J.-L. Bantignies, Chromophore Ordering by Confinement into Carbon Nanotubes, The Journal of Physical Chemistry C. 118 (2014) 19462–19468. doi:10.1021/jp505804d.

[12] M. Milko, P. Puschnig, C. Draxl, Predicting the electronic structure of weakly interacting hybrid systems: The example of nanosized peapod structures, Physical Review B. 86 (2012). doi:10.1103/PhysRevB.86.155416.

[13] T. Yumura, H. Yamashita, Modulating the Electronic Properties of Multimeric Thiophene Oligomers by Utilizing Carbon Nanotube Confinement, The Journal of Physical Chemistry C. 118 (2014) 5510–5522. doi:10.1021/jp5006555.

[14] H. Yamashita, T. Yumura, The Role of Weak Bonding in Determining the Structure of Thiophene Oligomers inside Carbon Nanotubes, The Journal of Physical Chemistry C. 116 (2012) 9681–9690. doi:10.1021/jp301972e.

[15] M. Milko, P. Puschnig, P. Blondeau, E. Menna, J. Gao, M.A. Loi, C. Draxl, Evidence of Hybrid Excitons in Weakly Interacting Nanopeapods, The Journal of Physical Chemistry Letters. 4 (2013) 2664–2667. doi:10.1021/jz401073t.

[16] W. Orellana, S.O. Vásquez, Endohedral terthiophene in zigzag carbon nanotubes: Density functional calculations, Physical Review B. 74 (2006). doi:10.1103/PhysRevB.74.125419.

[17] S. Niyogi, M.A. Hamon, H. Hu, B. Zhao, P. Bhowmik, R. Sen, M.E. Itkis, R.C. Haddon, Chemistry of Single-Walled Carbon Nanotubes, Accounts of Chemical Research. 35 (2002) 1105–1113. doi:10.1021/ar010155r.

[18] T. Saito, S. Ohshima, T. Okazaki, S. Ohmori, M. Yumura, S. Iijima, Selective Diameter Control of Single-Walled Carbon Nanotubes in the Gas-Phase Synthesis, Journal of Nanoscience and Nanotechnology. 8 (2008) 6153–6157. doi:10.1166/jnn.2008.SW23.

* laurent.alvarez@umontpellier.fr; 33 4 67 14 35 41

[19] B. Kitiyanan, W.E. Alvarez, J.H. Harwell, D.E. Resasco, Controlled production of single-wall carbon nanotubes by catalytic decomposition of CO on bimetallic Co–Mo catalysts, Chemical Physics Letters. 317 (2000) 497–503.
[20] O. Dubay, G. Kresse, H. Kuzmany, Phonon Softening in Metallic Nanotubes by a Peierls-like Mechanism, Physical Review Letters. 88 (2002). doi:10.1103/PhysRevLett.88.235506.
[21] S. Piscanec, M. Lazzeri, F. Mauri, A.C. Ferrari, J. Robertson, Kohn Anomalies and Electron-Phonon Interactions in Graphite, Physical Review Letters. 93 (2004). doi:10.1103/PhysRevLett.93.185503.
[22] M. Fouquet, H. Telg, J. Maultzsch, Y. Wu, B. Chandra, J. Hone, T.F. Heinz, C. Thomsen, Longitudinal Optical Phonons in Metallic and Semiconducting Carbon Nanotubes, Physical Review Letters. 102 (2009). doi:10.1103/PhysRevLett.102.075501.
[23] M. Lazzeri, F. Mauri, Nonadiabatic Kohn Anomaly in a Doped Graphene Monolayer, Physical Review Letters. 97 (2006). doi:10.1103/PhysRevLett.97.266407.
[24] P. Puech, T. Hu, A. Sapelkin, I. Gerber, V. Tishkova, E. Pavlenko, B. Levine, E. Flahaut, W. Bacsa, Charge transfer between carbon nanotubes and sulfuric acid as determined by Raman spectroscopy, Physical Review B. 85 (2012). doi:10.1103/PhysRevB.85.205412.
[25] A. Das, A.K. Sood, Renormalization of the phonon spectrum in semiconducting single-walled carbon nanotubes studied by Raman spectroscopy, Physical Review B. 79 (2009). doi:10.1103/PhysRevB.79.235429.
[26] J.C. Tsang, M. Freitag, V. Perebeinos, J. Liu, P. Avouris, Doping and phonon renormalization in carbon nanotubes, Nature Nanotechnology. 2 (2007) 725–730. doi:10.1038/nnano.2007.321.
[27] N. Caudal, A.M. Saitta, M. Lazzeri, F. Mauri, Kohn anomalies and nonadiabaticity in doped carbon nanotubes, Physical Review B. 75 (2007). doi:10.1103/PhysRevB.75.115423.
[28] D.I. Levshov, Y.I. Yuzyuk, T. Michel, C. Voisin, L. Alvarez, S. Berger, P. Roussignol, J.-L. Sauvajol, Raman Probing of Uniaxial Strain in Individual Single-Wall Carbon Nanotubes in a Composite Material, The Journal of Physical Chemistry C. 114 (2010) 16210–16214. doi:10.1021/jp1040635.
[29] A. Duzynska, M. Swiniarski, A. Wroblewska, A. Lapinska, K. Zeranska, J. Judek, M. Zdrojek, Phonon properties in different types of single-walled carbon nanotube thin films probed by Raman spectroscopy, Carbon. 105 (2016) 377–386. doi:10.1016/j.carbon.2016.04.064.
[30] B. Gao, L. Jiang, X. Ling, J. Zhang, Z. Liu, Chirality-Dependent Raman Frequency Variation of Single-Walled Carbon Nanotubes under Uniaxial Strain, The Journal of Physical Chemistry C. 112 (2008) 20123–20125. doi:10.1021/jp809374j.
[31] Z. Liu, J. Zhang, B. Gao, Raman spectroscopy of strained single-walled carbon nanotubes, Chemical Communications. (2009) 6902. doi:10.1039/b914588e.
[32] A. Merlen, N. Bendiab, P. Toulemonde, A. Aouizerat, A. San Miguel, J.L. Sauvajol, G. Montagnac, H. Cardon, P. Petit, Resonant Raman spectroscopy of single-wall carbon nanotubes under pressure, Physical Review B. 72 (2005). doi:10.1103/PhysRevB.72.035409.
[33] L. Kavan, L. Dunsch, H. Kataura, A. Oshiyama, M. Otani, S. Okada, Electrochemical Tuning of Electronic Structure of C_{60} and C_{70} Fullerene Peapods: In Situ Visible Near-Infrared and Raman Study, The Journal of Physical Chemistry B. 107 (2003) 7666–7675. doi:10.1021/jp035332f.
[34] S.-K. Joung, T. Okazaki, S. Okada, S. Iijima, Interaction between single-wall carbon nanotubes and encapsulated C60 probed by resonance Raman spectroscopy, Physical Chemistry Chemical Physics. 12 (2010) 8118. doi:10.1039/c000102c.
[35] Y. Chen, G. Royal, E. Flahaut, S. Cobo, V. Bouchiat, L. Marty, N. Bendiab, Light Control of Charge Transfer and Excitonic Transitions in a Carbon Nanotube/Porphyrin Hybrid, Advanced Materials. 29 (2017) 1605745. doi:10.1002/adma.201605745.
[36] A. Das, A.K. Sood, A. Govindaraj, A.M. Saitta, M. Lazzeri, F. Mauri, C.N.R. Rao, Doping in Carbon Nanotubes Probed by Raman and Transport Measurements, Physical Review Letters. 99 (2007). doi:10.1103/PhysRevLett.99.136803.
[37] S.D.M. Brown, A. Jorio, P. Corio, M.S. Dresselhaus, G. Dresselhaus, R. Saito, K. Kneipp, Origin of the Breit-Wigner-Fano lineshape of the tangential *G* -band feature of metallic carbon nanotubes, Physical Review B. 63 (2001). doi:10.1103/PhysRevB.63.155414.
[38] H. Kataura, Y. Kumazawa, Y. Maniwa, I. Umezu, S. Suzuki, Y. Ohtsuka, Y. Achiba, Optical properties of single-wall carbon nanotubes, Synthetic Metals. 103 (1999) 2555–2558.

* laurent.alvarez@umontpellier.fr; 33 4 67 14 35 41

[39] G. Gordeev, A. Setaro, M. Glaeske, S. Jürgensen, S. Reich, Doping in covalently functionalized carbon nanotubes: A Raman scattering study: Doping in covalently functionalized carbon nanotubes, Physica Status Solidi (b). 253 (2016) 2461–2467. doi:10.1002/pssb.201600636.
[40] H. Farhat, H. Son, G.G. Samsonidze, S. Reich, M.S. Dresselhaus, J. Kong, Phonon Softening in Individual Metallic Carbon Nanotubes due to the Kohn Anomaly, Physical Review Letters. 99 (2007). doi:10.1103/PhysRevLett.99.145506.
[41] K. Sasaki, H. Farhat, R. Saito, M.S. Dresselhaus, Kohn anomaly in Raman spectroscopy of single wall carbon nanotubes, Physica E: Low-Dimensional Systems and Nanostructures. 42 (2010) 2005–2015. doi:10.1016/j.physe.2010.03.007.
[42] M. Ouyang, Energy Gaps in "Metallic" Single-Walled Carbon Nanotubes, Science. 292 (2001) 702–705. doi:10.1126/science.1058853.
[43] R. Saito, M. Hofmann, G. Dresselhaus, A. Jorio, M.S. Dresselhaus, Raman spectroscopy of graphene and carbon nanotubes, Advances in Physics. 60 (2011) 413–550. doi:10.1080/00018732.2011.582251.
[44] R. Saito, A.R.T. Nugraha, E.H. Hasdeo, N.T. Hung, W. Izumida, Electronic and Optical Properties of Single Wall Carbon Nanotubes, Topics in Current Chemistry. 375 (2017). doi:10.1007/s41061-016-0095-2.
[45] X. Liu, H. Kuzmany, P. Ayala, M. Calvaresi, F. Zerbetto, T. Pichler, Selective Enhancement of Photoluminescence in Filled Single-Walled Carbon Nanotubes, Advanced Functional Materials. 22 (2012) 3202–3208. doi:10.1002/adfm.201200224.
[46] J. Campo, Y. Piao, S. Lam, C.M. Stafford, J.K. Streit, J.R. Simpson, A.R. Hight Walker, J.A. Fagan, Enhancing single-wall carbon nanotube properties through controlled endohedral filling, Nanoscale Horizons. 1 (2016) 317–324. doi:10.1039/C6NH00062B.
[47] A.V. Naumov, S.M. Bachilo, D.A. Tsyboulski, R.B. Weisman, Electric Field Quenching of Carbon Nanotube Photoluminescence, Nano Letters. 8 (2008) 1527–1531. doi:10.1021/nl0800974.
[48] A. Rakitin, C. Papadopoulos, J.M. Xu, Carbon nanotube self-doping: Calculation of the hole carrier concentration, Physical Review B. 67 (2003). doi:10.1103/PhysRevB.67.033411.
[49] K. Liu, M. Burghard, S. Roth, P. Bernier, Conductance spikes in single-walled carbon nanotube field-effect transistor, Applied Physics Letters. 75 (1999) 2494–2496. doi:10.1063/1.125059.
[50] M. Huang, Y. Wu, B. Chandra, H. Yan, Y. Shan, T.F. Heinz, J. Hone, Direct Measurement of Strain-Induced Changes in the Band Structure of Carbon Nanotubes, Physical Review Letters. 100 (2008). doi:10.1103/PhysRevLett.100.136803.
[51] S.D. Stranks, J.K. Sprafke, H.L. Anderson, R.J. Nicholas, Electronic and Mechanical Modification of Single-Walled Carbon Nanotubes by Binding to Porphyrin Oligomers, ACS Nano. 5 (2011) 2307–2315. doi:10.1021/nn103588h.
[52] A. Belhboub, P. Hermet, L. Alvarez, R. Le Parc, S. Rols, A.C. Lopes Selvati, B. Jousselme, Y. Sato, K. Suenaga, A. Rahmani, J.-L. Bantignies, Enhancing the Infrared Response of Carbon Nanotubes From Oligo-Quaterthiophene Interactions, The Journal of Physical Chemistry C. 120 (2016) 28802–28807. doi:10.1021/acs.jpcc.6b09329.

* laurent.alvarez@umontpellier.fr; 33 4 67 14 35 41